small NANO MICRO

Carbon-nanotube nanorings

Elastic Deformation of Carbon-Nanotube Nanorings

*Meng Zheng and Changhong Ke**

***A** combined experimental–theoretical study of the mechanical deformation of carbon-nanotube (CNT) nanorings is presented. The CNT ring employed is formed by folding a long and thin single-walled-CNT bundle. The mechanical deformations of the CNT ring when it is pushed against and pulled away from a flat substrate are experimentally characterized in situ, inside a high-resolution scanning electron microscope through nanomanipulation. The experimental measurements clearly reveal that the CNT ring displays a purely elastic behavior during multiple repeated large-displacement deformation processes. A theoretical model based on nonlinear elastica theory is used to quantitatively study the mechanical behavior of the CNT ring and to interpret the experimental results. This work shows for the first time that van der Waals interactions between the CNT ring and the substrate have significant effects on the ring's elastic deformation, including a bifurcation in its force–displacement profile. The results suggest that CNT nanorings can be used as ultrasensitive force sensors and flexible and stretchable structural components in novel nanoscale mechanical and electromechanical systems.*

Keywords:
- carbon nanotubes
- elastic deformation
- mechanical properties
- nanorings
- scanning electron microscopy

1. Introduction

Carbon nanotubes (CNTs) are a type of high-aspect-ratio, one-dimensional nanostructure with extraordinary mechanical, electrical, thermal, and chemical properties,[1–8] and hold promise for a number of applications, such as composites, sensors, and electronics.[9–11] Typically, individual or bundled CNTs stay in a straight or curved open fiber or rope configuration. Closed structures of CNTs, such as rings and tori, have been observed in both as-grown products and post-treated materials. Directly synthesized nanorings formed by individual or more commonly bundled single-walled,[12–15] double-walled,[16,17] triple-walled,[18] and much larger diameter multi-walled CNTs[19] have been reported. Recent work shows that CNT ring structures can be grown on a large scale by chemical vapor deposition with yields up to 50%.[20] By chemical modification of both ends of the CNTs, Sano et al. reported that open CNTs can form closed-ring structures due to the covalent bonding between the newly added functional groups at the CNT ends.[21] A long CNT fiber can self-fold to form a ring structure through overlapping part of its own structure.[22–24] This is due to the fact that the van der Waals interaction between CNT surfaces is strong enough to balance the mechanical deformation. This self-folding process can be facilitated by external excitation, such as ultrasonic agitation.[14,25]

Surface chemical functionalization is also used to assemble CNT ring structures on chemically patterned substrates.[26–28] Two nanotube-ring formation mechanisms are proposed based on previously reported modeling work on the formation, structure, and stability of the CNT nanoring.[29–38] The nanotube nanoring can be formed by either a hexagon structure with pentagon–heptagon defects, or by bending a defect-free CNT made of a pure hexagon network. It is believed that for nanorings with large ring diameters, the pure hexagon structure is energetically more stable and the ring curvature is accommodated by the bending of the nanotube, while for nanorings with small ring diameters, the mixture of hexagon and pentagon–heptagon defects is energetically more favorable with the ring curvature accommodated by pentagon–heptagon defects.

[*] Prof. C.-H. Ke, M. Zheng
Department of Mechanical Engineering
State University of New York at Binghamton
Binghamton, NY 13902 (USA)
E-mail: cke@binghamton.edu

Supporting Information is available on the WWW under http://www.small-journal.com or from the author.

DOI: 10.1002/smll.201000337

The unique topographical structure of CNT nanorings has prompted significant interest in studying their various physical properties and applications. The electrical conductance transport in CNT rings has been investigated[39–41] and their applications in electromagnetic devices, such as interferometer logic gates[42] and transistors,[43–45] have been proposed. Because CNTs are considered one of the strongest and most flexible molecular materials due to the hybridized sp^2 C–C covalent bonding and seamless hexagonal network architecture, it is reasonable to speculate that CNT rings can be used as load-bearing structural components for a number of applications, such as novel nanomechanical and nanoelectromechanical systems. However, to the best of our knowledge, no experimental and very few theoretical studies of the mechanical deformation of CNT rings[35] have been reported.

Herein, we present a combined experimental–theoretical study of the mechanical deformation of CNT nanorings. The CNT ring employed in our study was formed by mechanically folding a long and thin single-walled-CNT (SWNT) bundle. The mechanical deformations of the CNT ring on a flat substrate in both compression and tension were characterized in situ, inside a high-resolution scanning electron microscope through nanomanipulation. A theoretical model based on nonlinear elastica theory is employed to study the mechanical deformation of the CNT ring and to interpret the experimental measurements. The model takes into account the van der Waals interaction between the CNT ring and the substrate. Our results clearly show that this interaction has a profound impact on the elastic behavior of the CNT ring. Our work uniquely demonstrates that CNT rings are promising as novel force sensors or structural components in nanoscale mechanical and electromechanical systems.

2. Results and Discussion

2.1. In situ Electron Microscopy Experiments

The in situ experimental configuration for studying the mechanical deformation of a CNT ring is illustrated in Figure 1A (top view), in which one horizontally placed CNT ring is pushed against (or pulled away from) a vertically placed flat substrate by an external force *P*. In our experiments, one CNT ring is partially attached to the tungsten probe of a three-dimensional piezo-driven nanomanipulator, as exemplified by the sample shown in Figure 1B. The CNT ring of diameter 7.0 μm was formed by means of nanomanipulation to have one end portion of a thin, freestanding SWNT bundle attached to the central portion of the bundle and to fold into a closed ring-type structure. The freestanding SWNT bundles employed in this study were obtained by using our recently reported mechanical scratching approach.[46] The orientation of the manipulator probe was carefully adjusted so that the attached CNT ring stayed horizontal and its norm was parallel to the direction of the electron beam. The CNT ring was controlled with a nanometer resolution to approach a vertically placed Si substrate, which was coated with a 30-nm gold film and a 5-nm Cr adhesion layer by electron-beam evaporation. By slowly moving the manipulator probe toward the substrate, the mounted CNT ring was firstly controlled to push against the substrate until a significant deformation was reached. The manipulator probe was then controlled to slowly retract from the substrate and the compressive deformation of the CNT ring was gradually recovered. Due to the attractive van der Waals force between the CNT ring and the substrate, the CNT ring was still in contact with the substrate and its deformation was transformed into tensile deformation when the manipulator probe moved further away from the substrate. When the van der Waals force could not balance the pulling force on the CNT ring by the probe, the CNT ring was completely separated from the substrate and its tensile conformation was subsequently fully recovered.

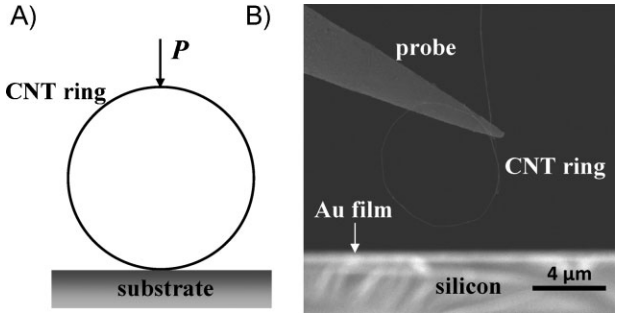

Figure 1. A) Schematic of a CNT ring on a flat substrate under a point load. B) SEM image of a folded CNT ring attached to a manipulator probe being positioned close to a vertically placed flat Si chip coated with a thin Au film.

We repeated the above pushing and pulling processes on the same CNT ring for two more cycles. The deformation curvatures of the CNT ring in each pushing and pulling position were captured by high-resolution scanning electron microscopy (HRSEM). The comparison between the geometrical shapes of the CNT ring before and after each pushing/pulling cycle reveals that no permanent shape change occurred after three repeated testing cycles, which strongly suggests that the deformation of the tested CNT ring was purely elastic. Four representative snapshots showing the deformation curvatures of the CNT ring in both compression and tension are presented in Figure 2. As expected, the vertical height of the ring decreased when it was under compressive load and increased when it was under tensile load. Because the CNT ring was placed at a lower horizontal plane than the top edge of the vertically placed substrate, the CNT ring and the top edge of the substrate could not be in focus with the electron beam at the same time, which resulted in the contact interface between the ring and substrate becoming a little blurred. Therefore, it is difficult to precisely quantify the length of the contact between the CNT ring and the substrate from the captured HRSEM images, which is also confirmed by our later analysis (Section 2.3). Nevertheless, we can reasonably speculate from the HRSEM images in Figure 2 that the contact length between the CNT ring and the substrate increased when it was pushed against the substrate and decreased when it was pulled away from the substrate.

It is noted that the attachment of the CNT ring on the tungsten probe during the whole pulling/pushing experiment was by van der Waals interaction only and no other fixture mechanism, such as electron-beam-induced hydrocarbon[47] or

NANO MICRO small

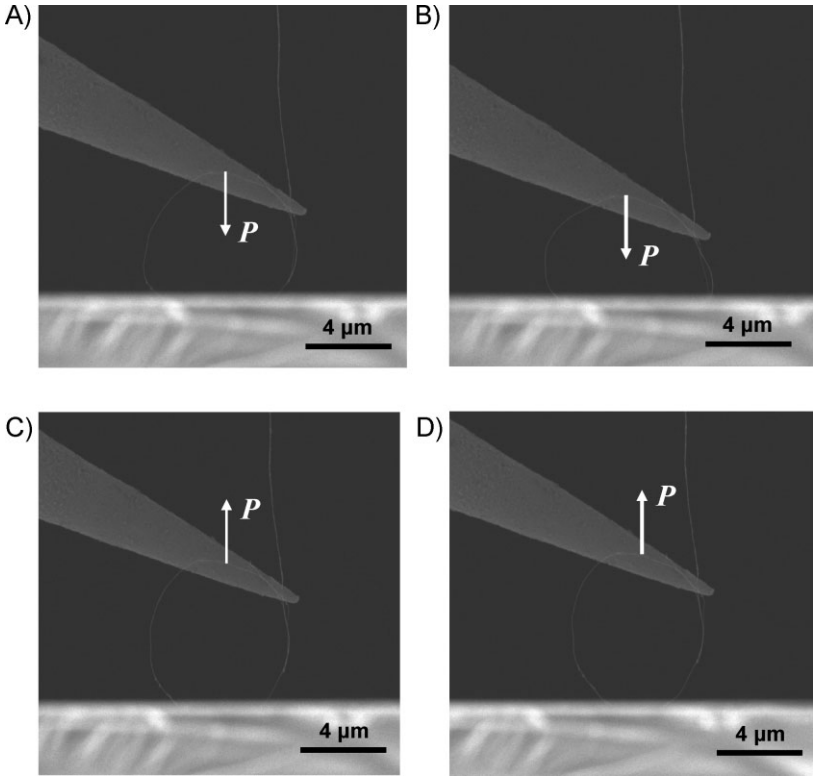

Figure 2. Selected SEM snapshots of the CNT ring shown in Figure 1B being pushed against the flat substrate (A,B) and pulled away from the flat substrate (C,D).

Pt[48] deposition, was employed. This observation suggests that the adhesion interaction between CNT and tungsten is strong enough to sustain the pushing and pulling forces exerted on the CNT ring by the manipulator probe, which are theoretically predicted to be in the sub-nN range using our nonlinear model (Section 2.3). Our analysis of the captured HRSEM images (see Figure S1 in the Supporting Information) also reveals that the portion of the CNT ring that was attached to the manipulator probe did not experience any visible deformation during the repeated pushing/pulling cycles. To the best of our knowledge, the in situ measurements presented here are the first reported experimental characterization of the mechanical deformation of CNT-based nanoring structures.

2.2. Nonlinear Elastica Modeling

In this section, we present a continuum model based on nonlinear elastica theory to study the mechanical deformation of the CNT ring in both compression and tension modes. In our model, the CNT ring is considered to be formed by bending an individual or bundled SWNT fiber such that both of its ends are connected directly, thus forming a closed-ring structure. The ring segment is theoretically modeled as an inextensible elastica rod.[46,49,50] This modeling assumption is consistent with the prior experimental observation that nanotubes could be repeatedly bent to large angles and strain without permanent distortion of the tube topography.[46,51]

The simplified CNT ring model is shown schematically in Figure 3A. To be consistent with our in situ experiments, segment EAF, which represents the ring segment attached to the probe, is considered to be rigid and the boundary conditions at points E and F are considered as fixed ends. It is noted that a flat segment of length $2a$ is considered in the model to account for the contact between the CNT ring and the substrate, and the minimal value of the contact length is considered to be the diameter of one carbon atom (0.142 nm),[52] while $a = 0$ when the CNT ring is fully separated from the substrate. The free-body diagram of segment DG is illustrated in Figure 3B, in which M, T, and V are the reaction moment, tensile force, and shear force on the rod cross section, respectively. The per-unit-length van der Waals (vdw) force f_{vdw} and energy W_{vdw} between the CNT ring and the substrate are calculated by using a continuum model[53] based on the Lennard-Jones potential,[54] which defines the potential between two atoms i and j as $\phi_{ij} = 4\varepsilon\left((\sigma/r_{ij})^{12} - (\sigma/r_{ij})^{6}\right)$, in which r_{ij} is the interatom distance, and ε and σ are material constants (for carbon–gold interactions, $\varepsilon = 0.01273$ eV and $\sigma = 2.9943$ Å[55]).

Here, we consider that the interaction between the CNT ring and the gold substrate is the weak adsorption-based interaction,[56] while ignoring possible strong chemical force

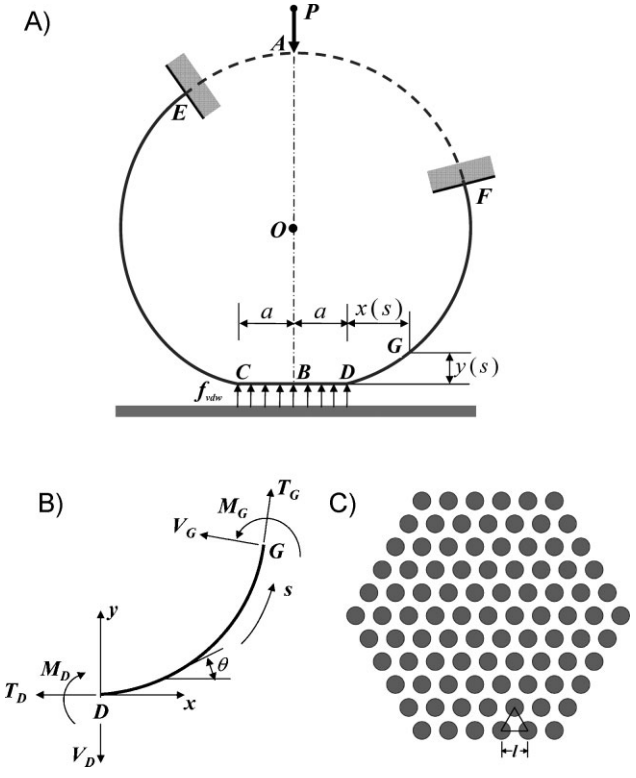

Figure 3. A) Schematic of the deformation of the CNT ring on a flat substrate. The dotted line represents the portion of the ring attached to the probe. B) Free-body diagram of one ring segment. C) Schematic of the postulated SWNT assembly configuration at the cross section of the tested CNT ring.

interaction between the nanotube and the gold substrate that was recently studied by González et al.[57] For simplification, we assume that the acting line of the external force P exerted on the CNT ring passes through the ring center O, and we also ignore the friction force between the CNT ring and the substrate. By considering our pushing/pulling experiments as quasi-static processes, we can obtain the following relationships:

$$V_D = V_C = f_{\mathrm{vdw}}(d_0) \cdot a = \frac{P}{2} \tag{1}$$

and

$$W_{\mathrm{vdw}}(d_0) = \frac{M_D^2}{2EI} = \frac{M_C^2}{2EI} \tag{2}$$

where d_0 is the gap distance between the lower fiber of the CNT ring and the substrate, and E and I are the Young's modulus and the moment of inertia of the bundled CNT, respectively. Equation (2) is derived based on the assumption that the separation of the CNT ring and the substrate at points C and D is due to the quasi-static balanced competition between the moment generated by the external load and the contact interfacial interaction between the CNT ring and the substrate.[50,58,59]

The elastic deformation of the CNT ring segment is given by:

$$\frac{\mathrm{d}^2\theta}{\mathrm{d}s^2} = \frac{T\sin\theta - V\cos\theta}{EI} \tag{3}$$

where s and θ are the arc length along the deformed ring segment and the angle between the slope of the curved ring segment and the x axis, respectively. The boundary conditions for the curved CNT ring segments DF at position D include $x_D = a, y_D = d_0, \theta_D = 0$, while at point F both x_F and θ_F are measured directly from the captured HRSEM images. Similar boundary conditions are also applied to segment EC. Considering $\mathrm{d}x = \cos\theta \mathrm{d}s$ and $\mathrm{d}y = \sin\theta \mathrm{d}s$, the exact deformation curvatures of the CNT ring in both compression and tension in the (x, y) coordinate system can be obtained numerically by solving Equations (1)–(3) using a shooting method. The detailed mathematical approach will be presented elsewhere[60] and here we will focus on presenting the major modeling results.

2.3. Comparison between Experimental Measurements and Theoretical Predictions

Based on the high-resolution transmission electron microscopy (HRTEM) characterization of thin SWNT bundles[46] prepared from the same sample batch as the SWNT bundle forming our tested CNT ring (see Figure S2 in the Supporting Information), the average radius of the nanotubes in the bundles is estimated to be ≈0.7 nm, which is close to that of (10,10) SWNTs ($R_{\mathrm{CNT}} = 0.678$ nm). Therefore, the radius of the tubes in the bundle forming our tested CNT ring as shown in Figure 1B is assumed to be equal to that of (10,10) tubes. It is worth mentioning that the assumed chirality of the tubes in our modeling is used to determine the radius of the nanotubes only. The lateral dimension of the CNT bundle is measured to be about 15 nm by HRSEM. Here we assume that the radial deformation of the tubes in the bundle due to the intertube van der Waals interaction is negligible[61] and the cross sections of the tubes remain circular, and that the tubes in the bundle form a hexagonal bundle cross section (see Figure 3C) with six tubes in contact with the substrate. The distance between the center of two neighboring tubes, or the triangular hexagon lattice, is calculated to be $l = 0.313 + 2R_{\mathrm{CNT}} = 1.67$ nm.[62] The height of the hexagon shown in Figure 3C is calculated to be 15.82 nm, which is close to our measured value (15 nm).

From the HRSEM images shown in Figures 1B and 2, we can see that there is a nanotube overlapping segment in the ring structure, the cross section of which most likely possesses a higher moment of inertia than the rest of the ring segment. Part of this nanotube overlapping segment is attached to the probe and is a fraction of the rigid segment EAF. Because the off-probe portion of the nanotube overlapping segment is only a small portion of the ring, we reasonably assume that its effect on the elastic behavior of the nanoring is negligible and consider a uniform cross section for the whole ring in our theoretical prediction, as illustrated in Figure 3C. The moment of inertia I of the bundle cross section is then calculated using the same approached as reported in Reference [46]. Using our nonlinear elastica model as presented in Section 2.2, the deformation curvatures of the tested CNT ring shown in Figure 1B under both compressive and tensile loads are obtained numerically.

Figure 4 shows four theoretically predicted deformation curvatures of the tested CNT ring, which respectively correspond to the four SEM snapshots shown in Figure 2. Each graphic in Figure 4 shows a comparison between the theoretical predictions and the experimental measurements on the deformation curvature of the CNT ring, the latter being measured directly from the respective HRSEM images. It can be clearly seen that the theoretical prediction and the experimental measurements on the deformation curvatures of the tested CNT ring are in good agreement, with the Young's modulus E of the SWNT as the only fitting parameter. All the simulation results presented herein are based on $E = 1.12$ TPa, which is consistent with previously reported values (1.0–1.2 TPa).[1] It is noted that the positions of the two end points of the ring segment attached to the probe, that is, points E and F, are measured directly from Figure 1B and the same values are employed in the theoretical predictions of the deformation curvatures shown in Figure 4A–D. For each deformation curvature, the external load applied on the CNT ring by the manipulator probe, which was not directly measured in our in situ experiments, is theoretically predicted and shown in the top-right corner of Figure 4A–D.

Figure 5A shows the relationship between the theoretically predicted applied load and the height of the CNT ring, L_{AB}, which is the measured vertical distance between points A and B from the HRSEM images, for three pushing/pulling cycles. Figure 5B shows the relationship between the applied load and the length of the flat contact between the CNT ring and the substrate. The solid curves in Figure 5A and B show the respective numerical results obtained by assuming that the

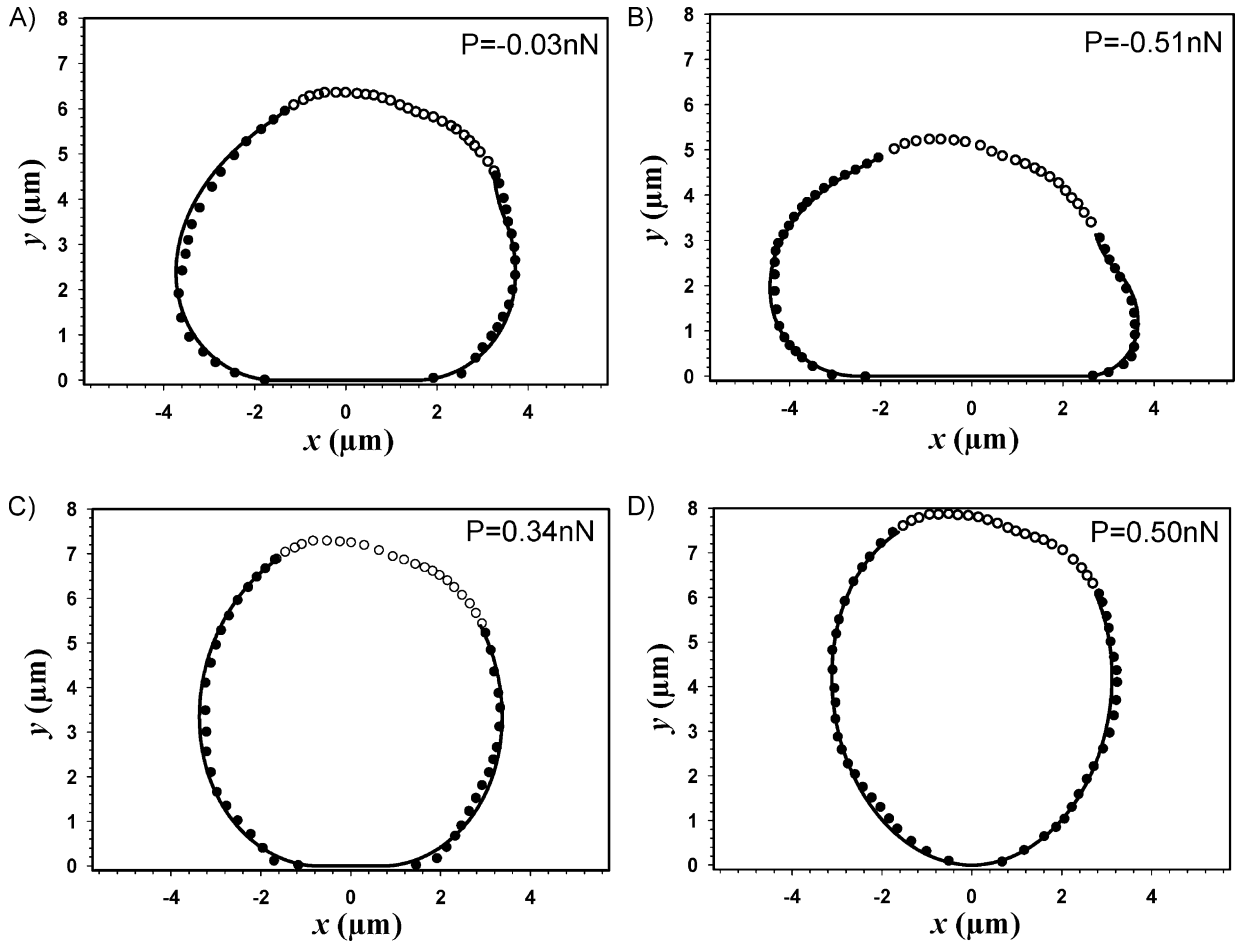

Figure 4. Comparison between experimental measurements and theoretical predictions on the four deformation curvatures shown in Figure 2. The solid-circle curve in each picture represents the experimental data measured from the respective HRSEM images, while the open-circle curve represents the experimental data for the portion of the CNT ring attached to the probe. The solid curve represents the theoretical predictions based on our nonlinear elastica model. The theoretically predicted applied load P is shown in each graphic.

CNT ring (shown in Figure 1B) is an ideal circular structure as illustrated in Figure 2A, in contrast to the discrete data shown in Figure 5A and B that are obtained by fitting the captured deformation curvatures using our model. It is noticed from Figure 5B that the theoretically predicted length of the flat contact is smaller than those observed from the respective SEM images (shown in Figure 3). This difference is due to the fact that the positions of the CNT ring and the edge of the substrate were not in the same horizontal level, such that the contact region between the CNT ring and the substrate was slightly out of focus when the CNT ring was in focus with the electron beam. Therefore, the length of the flat contact measured directly from the SEM images will be slightly overestimated.

The good agreement between experimental measurements and theoretical predictions suggests that 1) the mechanical deformation of the CNT ring under both compressive and tensile loads can be reasonably predicted by our nonlinear elastica model, as presented in Section 2.2; and 2) the SWNT assembly configuration in the bundle as shown in Figure 3C appears to be plausible. Figure 5A and B confirms our aforementioned statement that the large-displacement mechanical deformation of the CNT ring under compressive and tensile loads is purely elastic. From the experimental data shown in Figure 5B, the height of the CNT ring experienced a significant change ranging from −26 to 15% and no permanent deformation was observed after three repeated pushing/pulling cycles. Our theoretical modeling also reveals that the applied compressive and tensile loads on the tested CNT ring are in the sub-nN regime. The quantitative measurement of such tiny forces, even though not impossible, will be a significant challenge. Figure 5B shows that the magnitude of the pulling force is inversely correlated with the contact length, and the maximum pulling force occurs at very small contact length, while the magnitude of the pushing force is positively correlated with the contact length. This observation suggests that the change of the contact length between the nanotube ring and the substrate is a gradual pull-off or push-on process, which is strongly modulated by the deformation of the CNT ring structure that has a very small stiffness.

The maximum pulling force to lift the CNT ring from the substrate is estimated to be 0.54 nN and the corresponding contact length $2a = 30$ nm, as shown in Figure 5A and B. As mentioned in Section 2.2, the interaction between the nanotubes and the gold substrate is considered to be weak adsorption-based van der Waals interaction, and the nanotubes in contact with the gold film possess their pristine hybridized sp^2

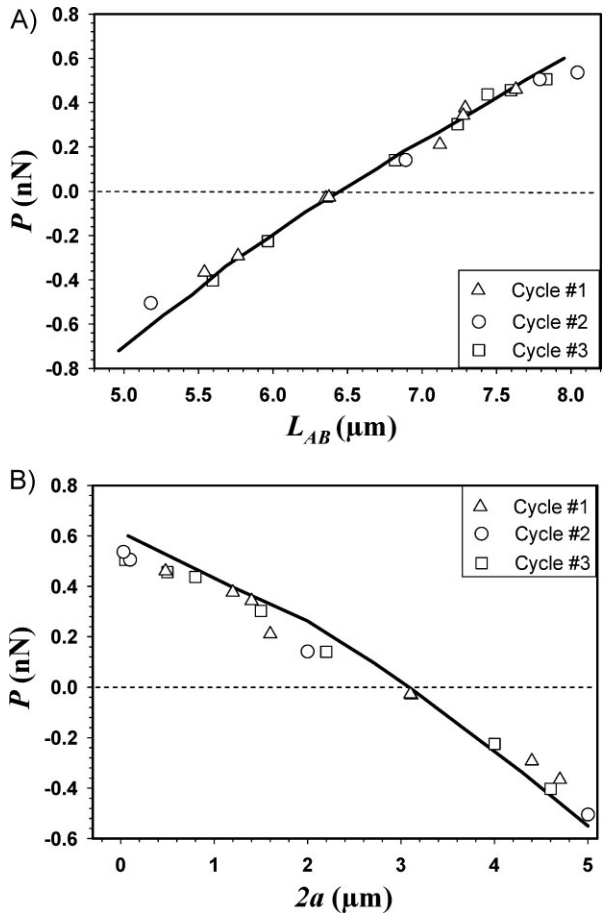

Figure 5. A) Relationship between the theoretically predicted applied load and the experimentally measured ring height. B) Relationship between the theoretically predicted applied load and the length of the flat contact of the tested CNT ring for three repeated pushing/pulling cycles.

C–C covalent network. The gold substrate employed in our measurements has a surface roughness (root mean square) of 2.0 nm for a $1 \times 1\ \mu m^2$ area and the surface gold atoms are in the form of the grain morphology (see Figure S3 in the Supporting Information). Because the gold film is much softer than the CNT, the high local contact stress will most likely first deform the gold film, and the nanotube hybridized sp^2 network in the contact interface is assumed to remain intact. It is noted that the carbon atoms in the nanotube of sp^2 hybridization could be converted to chemically more active sp^3 hybridization by high local distortion stress exerted by sharp atomic force microscopy (AFM) tips.[63,64] The nanotubes of hybridized sp^3 carbon atoms can form strong short-range chemical-bonding interactions with the gold substrate, which can be captured by AFM-based chemical force microscopy.[65,66]

Recently, González and co-workers reported a combined experimental–theoretical study of the chemical force between the gold-coated sharp AFM probe and individual SWNTs lying on a silicon oxide substrate.[57] Their experimentally measured adhesion force between the gold layer coated on the AFM probe and the nanotube was about 2 nN, which is in very good agreement with their theoretical predictions based on density functional theory (DFT). The difference between González's results and ours can be ascribed to two factors. One is the type of electron orbital hybridization of the carbon atoms in the nanotubes that are in direct contact with the gold film and the corresponding strength of the respective adhesion interaction. We have to point out that the roughness of the gold surface employed in our experiments may play an important role in the nanotube–gold surface interaction, which makes the precise theoretical prediction of the adhesion interaction much more complicated and requires sophisticated atomistic-level modeling approaches, such as the DFT used in González's work and molecular dynamics (MD). The actual pulling force in our system may be underestimated by our use of a model that ignores the possible strong chemical force interaction as revealed by González et al. The other factor is the difference between the pulling systems. For the system reported in González's work, the gold-coated AFM tip essentially has a nearly fixed-area contact with the nanotube during the pulling process, whereas in our system the contact length (area) between the CNT ring and the substrate decreases dramatically during the pulling process due to the strong modulating effect of the CNT ring deformation, as discussed earlier. The maximum per-unit-length attractive force between the bundled CNT as illustrated in Figure 3C and the gold substrate is calculated to be $0.28\ N\ m^{-1}$ (see Figure S4 in the Supporting Information). However, the per-unit-length van der Waals force when the CNT ring is closed for separation from the substrate is merely $0.018\ N\ m^{-1}$, while the total pulling force calculated by $P = q_{vdw} \times 2a$ reaches its maximum (0.54 nN). Our results reveal a very small variation of the gap size during this pulling process (see Figure S5 in the Supporting Information). Our results also show that for the moment when q_{vdw} reaches its maximum ($0.28\ N\ m^{-1}$), the calculated pulling force is actually quite small (0.05 nN) as a result of the very small flat contact length (0.19 nm), as presented later in Figure 6C. We argue that the second factor is the major reason accounting for the difference in the pulling force between our system and the system reported by González et al.

2.4. Mechanical Deformation of the CNT Ring on the Flat Substrate

It can be seen from Figure 5A and B that, under a very small external load of 30 pN, the tested CNT ring was under significant deformation (e.g., the height reduced by about 9%) and had a flat segment of 3.1 μm in contact with the substrate. This observation suggests that, even when no external force is applied, significant deformation of the CNT ring may occur when it stands vertically on a flat substrate. The mechanical deformation of the CNT ring under such load-free conditions is purely due to its van der Waals interaction with the substrate. To understand the effect of the van der Waals interaction on the deformation of the CNT ring, we theoretically modeled the elastic deformation of a perfectly circular ring made of SWNTs on a flat substrate. To facilitate comparison with the data shown in Figures 4 and 5, we employed all the parameters of the tested CNT ring shown in Figure 1B and the substrate used in the numerical simulations presented in Section 2.3.

Instead of having the CNT ring mounted to a probe, we consider that a point load is applied on the top of the ring, as

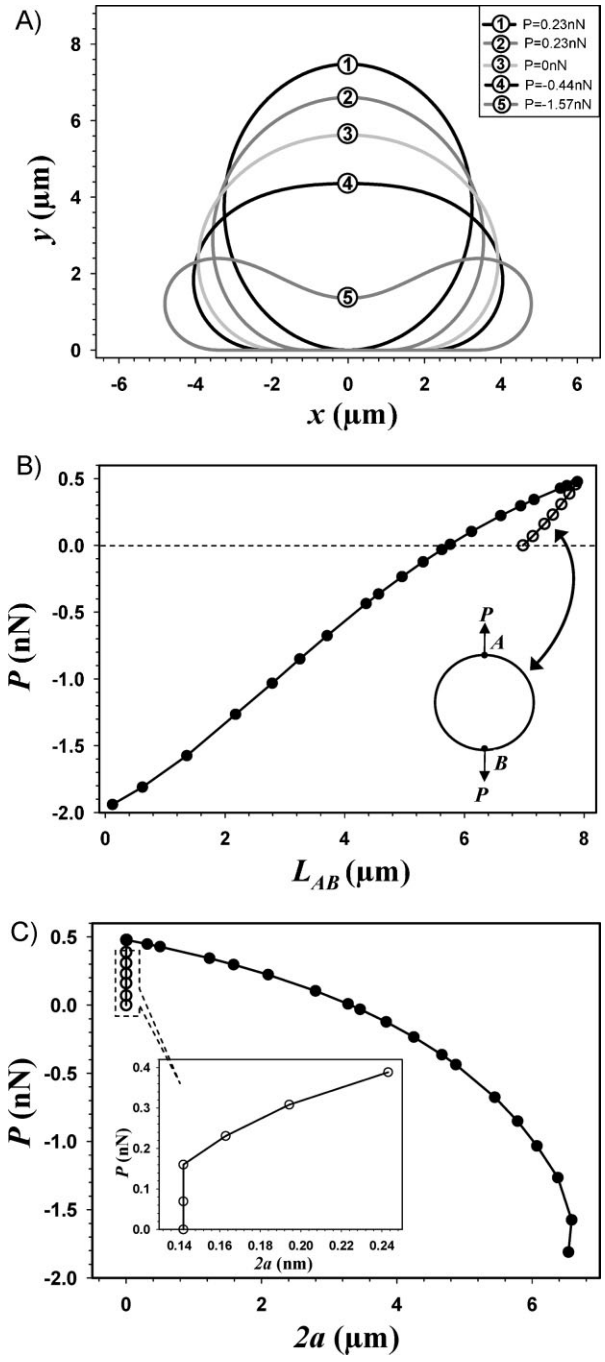

Figure 6. A) Selected theoretically predicted deformation curvatures of the perfectly circular CNT ring under point loads. B) Relationship between the theoretically predicted applied load and the height of the tested CNT ring. C) Relationship between the theoretically predicted applied load and the length of the flat contact.

illustrated in Figure 1A. In such a model, the full length of the CNT ring can deform as an inextensible elastica rod. Our theoretical modeling work[60] shows that the CNT ring will have a flat contact with the substrate if the ring radius exceeds a threshold value $R_{\min}$ that is given by $R_{\min} = \sqrt{\frac{EI}{2W_{vdw}}}$. Otherwise, the CNT ring will remain a perfectly circular structure and maintain a point contact with the substrate. Similar phenomena have been reported in previous studies of the radial deformation of individual SWNTs on a flat substrate[67] or between two neighboring SWNTs,[61] which are purely due to the van der Waals interactions. The reason that the CNT ring may remain a perfectly circular structure on a flat substrate is due to the fact that the CNT ring employed in our study is not internal force free in its undeformed configuration, and an internal bending moment is accommodated by its circular structure. For the CNT ring considered here, EI and W_{vdw} are calculated to be 2.31×10^{-21} N m^2 and 2.88×10^{-10} J m^{-1}, respectively. The corresponding threshold ring radius for having a flat contact with the substrate is calculated to be $R_{\min} = 2.0\,\mu$m, which is substantially lower than the ring radius of 3.5 μm for our tested CNT ring. Therefore, it is reasonable that the CNT ring shown in Figure 1B has a flat contact with the substrate under external force-free conditions.

Figure 6A shows several selected deformation curvatures of the perfectly circular CNT ring under zero-force, compressive, and tensile loads. As expected, when the CNT ring is in compression, an inflexion point is exhibited in its deformation curvature when the load exceeds a certain value. Figure 6B shows the relationship between the applied load and the height of the perfectly circular CNT ring, which displays an interesting bifurcation when the CNT is subjected to the tensile load. This bifurcation indicates that each applied tensile load corresponds to two equilibrium deformation curvatures for the same CNT ring, which have different heights and lengths of the flat contact with the substrate as shown in Figure 6B and C. It is noted that curves 1 and 2 in Figure 6A show the deformation curvatures of the CNT ring under the same applied load ($P = 0.23$ nN). The corresponding gap between the CNT ring and the substrate is 0.350 and 0.276 nm, respectively, while the respective height/length of the contact with the substrate is calculated to be 7.48 μm/0.16 nm and 6.61 μm/2.10 μm. When the CNT ring is subjected to compressive loads, both the force–height and force–length of the flat contact profiles shown in Figure 6B and C, respectively, display a simple monotonous relationship. The observed bifurcation for the CNT ring in tension is due to the fact that the employed van der Waals potential has a bifurcation in the attractive force region, while displaying a monotonous curve in the repulsive force region.

Our analysis shows that the force–height profile presented in Figure 5A obtained from our tested CNT corresponds to the solid-circle branch of the bifurcation shown in Figure 6B, while the open-circle branch was not captured by our in situ measurements. The majority of the solid-circle branch corresponds to a line contact between the CNT ring and the substrate, while a nearly point contact for the open-circle branch is observed. Our analysis further reveals that the open-circle branch is actually identical to the force–deformation profile of a perfectly circular CNT ring under two point loads, as illustrated by the inset in Figure 6B. The deformation curvature of the CNT ring under two point loads can be modeled by using nonlinear elastica theory and its analytical solutions are reported in Reference [68]. The open-circle branch of the bifurcation may be captured experimentally if additional constraints are imposed on the contact between the CNT ring and the substrate, such as the lower point of the CNT ring always being in subnanometer contact with the substrate. Even

though the effects of the van der Waals interaction on the deformation of the CNT have been extensively studied by a variety of continuum and atomistic modeling techniques,[23,24,61,69–71] to the best of our knowledge our finding of a bifurcation in the CNT ring elastic profile due to the van der Waals interaction is the first of its kind and will be useful in the pursuit of novel bistable, load-bearing components based on CNT nanorings.

It is worth mentioning that the nonlinear elastica model presented herein does not take into account possible buckling or rippling of the nanotube in the ring structure, as suggested by prior continuum and atomistic modeling studies.[32,34] When buckling occurs, the ring actually becomes polygon shaped. The buckling of the CNT depends on the ratio between the ring radius R and the CNT radius R_{CNT}. To keep a circular shape, Hod et al.[32] showed that the CNT ring radius $R \geq \frac{n^2}{2} R_{CNT}$, where n is a tube-chirality-dependent integer and can be determined from MD simulations. For CNT rings made of individual (10,10) tubes, we find that $n = 8$.[35,60] For our tested CNT ring, the radius of the CNT bundle is calculated to be 9.7 nm, which results in $R/R_{CNT} = 361$. Therefore, it is reasonable to consider that our tested CNT ring is a circular structure and its mechanical deformation can be theoretically obtained by using the nonlinear elastica model presented in Section 2.2.

The relationship between the applied load and the height of the ring shown in Figure 6B displays a nearly linear correlation for the height ranging from 5.6 μm ($P = 0$) to 1.4 μm ($P = -1.5$ nN). If we consider the stiffness or spring constant of the CNT ring is defined as $k = \frac{\Delta P}{\Delta L_{AB}}$, for the CNT ring studied herein $k = 0.36$ pN nm^{-1}, which suggests that CNT rings can act as an ultrasensitive force sensor as well as novel flexible and stretchable structural components in nanoscale mechanical and electromechanical systems. The CNT ring–substrate system presented will also be useful to quantitatively measure the surface energy of solid substrates and the binding energy between CNTs and solid substrates, provided that the geometrical information of the CNT in the ring structure and the applied load are known. Such techniques have been previously employed to characterize the surface energy on the macroscale.[72] We want to highlight the fact that, for the pursuit of the above-mentioned applications and performance optimization, it is essential to understand the effects of the intrinsic quantities of the nanotube ring, and the interaction strength between the nanotube and the substrate, on the elastic behavior of the nanoring. A systematic and parametric study on this important issue is currently in progress and will be reported in a future publication.

3. Conclusions

We have presented a combined experimental–theoretical study of the mechanical deformation of CNT nanorings. The mechanical deformations of the CNT ring when it was pushed against and pulled away from a flat substrate were experimentally characterized in situ, inside a high-resolution scanning electron microscope through nanomanipulation. Our experimental measurements clearly reveal that the CNT ring displays purely elastic behavior even when it experiences multiple repeated large-displacement deformations. A nonlinear elastica-based theoretical model is employed to quantitatively study the mechanical behavior of the CNT ring and to interpret the experimental results. Our combined experimental–theoretical work shows that van der Waals interactions between the CNT ring and the substrate have significant effects on the mechanical deformation of the ring. The observed bifurcation in the force–deformation profile of the CNT ring is discussed. The results suggest that CNT rings hold promise for ultrasensitive force sensors and novel flexible and stretchable structural components in nanoscale mechanical and electromechanical systems.

Acknowledgements

This work was supported by the State University of New York at Binghamton, and was partially supported by the American Chemical Society–Petroleum Research Fund. We thank Dr. In-Tae Bae and Dr. Guangwen Zhou for their assistance in the TEM characterization and many helpful discussions. The in situ scanning electron microscopy measurements were performed using the facilities in the Analytical and Diagnostics Laboratory at Binghamton University's Small Scale Systems Integration and Packaging Center (S^{3}IP).

[1] *Carbon Nanotubes*, (Eds: M. S. Dresselhaus, G. Dresselhaus, P. Avouris), Springer, Berlin **2001**.
[2] J. Y. Huang, S. Chen, Z. Q. Wang, K. Kempa, Y. M. Wang, S. H. Jo, G. Chen, M. S. Dresselhaus, Z. F. Ren, *Nature* **2006**, *439*, 281.
[3] D. Qian, G. J. Wagner, W. K. Liu, M. F. Yu, R. S. Ruoff, *Appl. Mech. Rev.* **2002**, *55*, 495.
[4] B. Liu, H. Jiang, H. T. Johnson, Y. Huang, *J. Mech. Phys. Solids* **2004**, *52*, 1.
[5] T. Lin, V. Bajpai, T. Ji, L. M. Dai, *Aust. J. Chem.* **2003**, *56*, 635.
[6] H. Jiang, B. Liu, Y. Huang, K. C. Hwang, *J. Eng. Mater. Technol. ASME* **2004**, *126*, 265.
[7] J. Hone, M. C. Llaguno, M. J. Biercuk, A. T. Johnson, B. Batlogg, Z. Benes, J. E. Fischer, *Appl. Phys. A Mater. Sci. Process.* **2002**, *74*, 339.
[8] D. Tasis, N. Tagmatarchis, A. Bianco, M. Prato, *Chem. Rev.* **2006**, *106*, 1105.
[9] H. G. Craighead, *Science* **2000**, *290*, 1532.
[10] B. Mahar, C. Laslau, R. Yip, Y. Sun, *IEEE Sensors J.* **2007**, *7*, 266.
[11] J. N. Coleman, U. Khan, Y. K. Gun'ko, *Adv. Mater.* **2006**, *18*, 689.
[12] L. Song, L. J. Ci, L. F. Sun, C. H. Jin, L. F. Liu, W. J. Ma, D. F. Liu, X. W. Zhao, S. D. Luo, Z. X. Zhang, Y. J. Xiang, J. J. Zhou, W. Y. Zhou, Y. Ding, Z. L. Wang, S. S. Xie, *Adv. Mater.* **2006**, *18*, 1817.
[13] L. Song, L. J. Ci, C. H. Jin, P. H. Tan, L. F. Sun, W. J. Ma, L. F. Liu, D. F. Liu, Z. X. Zhang, Y. J. Xiang, S. D. Luo, X. W. Zhao, J. Shen, J. J. Zhou, W. Y. Zhou, S. S. Xie, *Nanotechnology* **2006**, *17*, 2355.
[14] R. Martel, H. R. Shea, P. Avouris, *J. Phys. Chem. B* **1999**, *103*, 7551.
[15] R. Martel, H. R. Shea, P. Avouris, *Nature* **1999**, *398*, 299.
[16] J. F. Colomer, L. Henrard, E. Flahaut, G. Van Tendeloo, A. A. Lucas, P. Lambin, *Nano Lett.* **2003**, *3*, 685.
[17] X. H. Zhong, Y. L. Li, F. Hou, J. M. Feng, *Appl. Phys. A Mater. Sci. Process.* **2008**, *92*, 709.
[18] H. Yu, Q. F. Zhang, G. H. Luo, F. Wei, *Appl. Phys. Lett.* **2006**, *89*, 223106.

[19] M. Ahlskog, E. Seynaeve, R. J. M. Vullers, C. Van Haesendonck, A. Fonseca, K. Hernadi, J. B. Nagy, *Chem. Phys. Lett.* **1999**, *300*, 202.
[20] Z. P. Zhou, D. Y. Wan, Y. Bai, X. Y. Dou, L. Song, W. Y. Zhou, Y. J. Mo, S. S. Xie, *Physica E* **2006**, *33*, 24.
[21] M. Sano, A. Kamino, J. Okamura, S. Shinkai, *Science* **2001**, *293*, 1299.
[22] M. J. Buehler, Y. Kong, H. J. Gao, *J. Eng. Mater. Technol. ASME* **2004**, *126*, 245.
[23] M. J. Buehler, Y. Kong, H. Gao, Y. Huang, *J. Eng. Mater. Technol.* **2006**, *128*, 3.
[24] M. J. Buehler, *J. Mater. Res.* **2006**, *21*, 2855.
[25] S. W. Liu, J. J. Zhu, Y. Mastai, I. Felner, A. Gedanken, *Chem. Mater.* **2000**, *12*, 2205.
[26] S. L. Zou, D. Maspoch, Y. H. Wang, C. A. Mirkin, G. C. Schatz, *Nano Lett.* **2007**, *7*, 276.
[27] Y. H. Wang, D. Maspoch, S. L. Zou, G. C. Schatz, R. E. Smalley, C. A. Mirkin, *Proc. Natl. Acad. Sci. USA* **2006**, *103*, 2026.
[28] S. Motavas, B. Omrane, C. Papadopoulos, *Langmuir* **2009**, *25*, 4655.
[29] D. H. Oh, J. M. Park, K. S. Kim, *Phys. Rev. B* **2000**, *62*, 1600.
[30] M. Huhtala, A. Kuronen, K. Kaski, *Comput. Phys. Commun.* **2002**, *147*, 91.
[31] M. Huhtala, A. Kuronen, K. Kaski, *Comput. Phys. Commun.* **2002**, *146*, 30.
[32] O. Hod, E. Rabani, R. Baer, *Phys. Rev. B* **2003**, *67*, 195408.
[33] J. Han, *Chem. Phys. Lett.* **1998**, *282*, 187.
[34] L. Liu, C. S. Jayanthi, S. Y. Wu, *Phys. Rev. B* **2001**, *6403*, 033412.
[35] C. Feng, K. M. Liew, *Carbon* **2009**, *47*, 3508.
[36] V. Meunier, P. Lambin, A. A. Lucas, *Phys. Rev. B* **1998**, *57*, 14886.
[37] S. L. Zhang, S. M. Zhao, M. G. Xia, E. H. Zhang, T. Xu, *Phys. Rev. B* **2003**, *68*, 245419.
[38] P. Liu, Y. W. Zhang, C. Lu, *Phys. Rev. B* **2005**, *72*, 115408.
[39] M. Eroms, L. Mayrhofer, M. Grifoni, *Phys. Rev. B* **2008**, *78*, 075403.
[40] S. Latil, S. Roche, A. Rubio, *Phys. Rev. B* **2003**, *67*, 165420.
[41] F. L. Hu, H. T. Yang, X. P. Yang, J. M. Dong, *Phys. Rev. B* **2006**, *73*, 235437.
[42] J. Yi, G. Cuniberti, *Ann. NY Acad. Sci.* **2003**, *1006*, 306.
[43] H. Watanabe, C. Manabe, T. Shigematsu, M. Shimizu, *Appl. Phys. Lett.* **2001**, *78*, 2928.
[44] H. Watanabe, K. Shimotani, T. Shigematu, C. Manabe, *Thin Solid Films* **2003**, *438*, 462.
[45] G. Cuniberti, J. Y. Yi, M. Porto, *Appl. Phys. Lett.* **2002**, *81*, 850.
[46] C. Ke, M. Zheng, G. Zhou, W. Cui, N. Pugno, R. N. Miles, *Small* **2010**, *6*, 438.
[47] C. H. Ke, H. D. Espinosa, *Small* **2006**, *2*, 1484.
[48] C. H. Ke, N. Pugno, B. Peng, H. D. Espinosa, *J. Mech. Phys. Solids* **2005**, *53*, 1314.
[49] Y. Mikata, *Acta Mechanica* **2007**, 190. 133.
[50] C-H Ke, M Zheng, I.-T Bae, G.-W. Zhou, *J. Appl. Phys.* **2010**, *107*, 104305.
[51] M. R. Falvo, G. J. Clary, R. M. Taylor, V. Chi, F. P. Brooks, S. Washburn, R. Superfine, *Nature* **1997**, *389*, 582.
[52] T. Vodenitcharova, L. C. Zhang, *Phys. Rev. B* **2003**, *68*, 165401.
[53] M. Dequesnes, S. V. Rotkin, N. R. Aluru, *Nanotechnology* **2002**, *13*, 120.
[54] J. E. Lennard-Jones, *Proc. R. Soc. A* **1930**, *129*, 598.
[55] W. D. Luedtke, U. Landman, *Phys. Rev. Lett.* **1999**, *82*, 3835.
[56] A. Maiti, A. Ricca, *Chem. Phys. Lett.* **2004**, *395*, 7.
[57] C. González, J. Ortega, F. Flores, D. Martinez-Martin, J. Gomez-Herrero, *Phys. Rev. Lett.* **2009**, *102*, 106801.
[58] L. D. Landau, E. M. Lifshitz, *Theory of Elasticity*, Pergamon, Oxford **1986**.
[59] O. A. Goussev, P. Richner, U. W. Suter, *J. Adhes.* **1999**, *69*, 1.
[60] M. Zheng, C. Ke, unpublished.
[61] T. Tang, A. Jagota, C. Y. Hui, *J. Appl. Phys.* **2005**, *97*, 074304.
[62] L. A. Girifalco, M. Hodak, R. S. Lee, *Phys. Rev. B* **2000**, *62*, 13104.
[63] T. W. Tombler, C. W. Zhou, L. Alexseyev, J. Kong, H. J. Dai, L. Lei, C. S. Jayanthi, M. J. Tang, S. Y. Wu, *Nature* **2000**, *405*, 769.
[64] H. W. C. Postma, T. Teepen, Z. Yao, M. Grifoni, C. Dekker, *Science* **2001**, *293*, 76.
[65] R. Garcia, R. Perez, *Surf. Sci. Rep.* **2002**, *47*, 197.
[66] F. J. Giessibl, *Rev. Mod. Phys.* **2003**, *75*, 949.
[67] T. Hertel, R. E. Walkup, P. Avouris, *Phys. Rev. B* **1998**, *58*, 13870.
[68] R. Frisch-Fay, *Flexible Bars*, Butterworths, London **1962**.
[69] Z. L. Li, P. Dharap, S. Nagarajaiah, R. P. Nordgren, B. Yakobson, *Int. J. Solids Structures* **2004**, *41*, 6925.
[70] W. Zhou, Y. Huang, B. Liu, J. Wu, K. C. Hwang, B. Q. Wei, *Nano* **2007**, *2*, 175.
[71] W. Zhou, Y. Huang, B. Liu, K. C. Hwang, J. M. Zuo, M. J. Buehler, H. Gao, *Appl. Phys. Lett.* **2007**, *90*, 073107.
[72] J. Qi, D. A. Dillard, R. H. Plaut, J. G. Dillard, *J. Adhes.* **2003**, *79*, 559.

Received: March 2, 2010
Revised: April 20, 2010
Published online: July 7, 2010

